

Evidence Based Feature Selection and Collaborative Representation Towards Learning Based PSF Estimation for Motion Deblurring

Rohan Raju Dhanakshirur
Indian Institute of Technology, New Delhi
rohandhanakshirur@gmail.com

Ujwala Patil
KLE Technological University, Hubballi
ujwalapatil@kletech.ac.in

Ramesh Ashok Tabib
KLE Technological University, Hubballi
rameshashoktabib@gmail.com

Uma Mudenagudi
KLE Technological University, Hubballi
uma@kletech.ac.in

Abstract

The motion blur in an image is due to the relative motion between the camera and the scene being captured. Due to the degraded quality of the motion-blurred images, it is challenging to use them in different applications such as text detection, scene understanding, content-based image retrieval, etc. Typically, a motion-blurred image is modeled as a convolution between the un-blurred image and a Point Spread Function (PSF). Motion de-blurring is sensitive to the estimated PSF. In this paper, we propose to address the problem of motion deblurring by estimating PSF using a learning-based approach. We model motion blur as a function of length and angle and propose to estimate these parameters using a learning-based framework. It is challenging to find distinct features to precisely learn the extent of motion blur through deep learning. To address this, we model an evidence-based technique to select the relevant features for learning from a set of features, based on the confidence generated by combining the evidences using Dempster Shafer Combination Rule (DSCR). We propose to use Clustering and Collaborative Representation (CCR) of feature spaces to learn length and angle. We model the de-blurred image as an MRF (Markov Random Field) and use MAP (maximum a posteriori) estimate as the final solution. We demonstrate the results on real and synthetic datasets and compare the results with different state of art methods using various quality metrics and vision tools.

Index terms— Image restoration, motion deblurring, Point Spread Function (PSF), Dempster Shafer Combination Rule (DSCR), Clustering and Collaborative Representation (CCR), maximum a posteriori (MAP) estimate.

1. Introduction

The degradation of the image takes place due to the advent of blur and noise on the true (un-blurred) image. Motion blur occurs due to the relative motion between camera and the scene. Typically, blurred image is modelled as a convolution of un-blurred image and the motion PSF. Image deblurring is a process of reconstructing true image from the degraded image. The process of image deblurring is challenging due to the unknown PSF. Various methods are proposed in literature to perform image deblurring.

Image deblurring algorithms can be classified into two categories based on the approach used to restore the image [32]. The first category of algorithms perform PSF estimation and image restoration simultaneously. The second category of algorithms demand estimation of the PSF first to apply classical deconvolution methods.

Numerous methods [16], [2], [23], [22] which perform PSF estimation and image restoration simultaneously, assume sparsity of image gradients. These are widely used in trivial vision tasks including denoising, stereo, and optical flow. However, authors in [22] show, deblurring methods based on image gradients tend to favor blurry images over clear images, especially for algorithms formulated within the maximum a posterior (MAP) framework. To overcome this problem, authors in [9], [43] discuss a heuristic edge selection to achieve better results in the MAP framework. Natural image priors such as normalized sparsity prior [20], L0-regularized prior [44], and internal patch recurrence [24] are also introduced to favour true images instead of blurred ones. However, these natural image models do not generalize well for specific images such as face [30], text [6], [8], [31], and low illumination [17] images.

A large class of deblurring algorithms use the Total Variation (TV)-type priori [4], [41], [29]. They mostly differ in the optimization method used for solving the resulting

cost function and specific definition of the TV term. Other methods take advantage of nonlocal differential operator as the prior with different norms [45], [51], [38]. Sparse representation of images in some appropriate domain is also done in different sparsity-based methods [27], [13]. In [21], Hessian norm priori is used for deblurring with biomedical applications. Authors in [28] use example-based manifold priors. A progressive intra-scale, inter-scale approach is used in [49] for non-blind image deconvolution. Authors in [36] have proposed a cost function that involves data fidelity term with different derivative terms for motion de-blurring of natural images. The challenge with these algorithms is, the regularization parameter controls the final estimate from being too smooth or exhibiting unpleasant noise amplification and ringing artifacts [18].

Authors in [1], [3], [42], [7] and [14] propose to estimate the PSF and then apply classical de-convolution process. Authors in [40] propose an algorithm that uses the Harr wavelet transform (HWT) in discriminating different types of edges in order to determine the extent of blur in an image. Authors in [1] propose to transform image in cepstrum domain to estimate the motion blur kernel. Authors in [19] use Radon transform to obtain the properties of motion blur in cepstral analysis. Authors in [46] estimate extent of motion blur with the help of periodic patterns in frequency spectrum. They propose blur direction identification using Hough transform and blur length estimation by collapsing the 2D spectrum into 1D spectrum. Authors in [15] propose another method consisting of Hanning window and histogram equalization as pre-processing steps. They apply Hanning window to remove boundary artifacts and also improve the contrast of the image by performing histogram equalization. Rekleities [35] use steerable filter to detect the motion blur angle corresponding to maximum response of gradients. Chang et al. [3] makes use of bispectrum to detect motion blur parameters. Yoshida et al. [48] present a method using Discrete Cosine Transform (DCT) of image to detect uniform motion blur parameters.

Above methods are sensitive to the estimation of motion blur parameters. To address this, authors in [10] discuss a learning based approach to determine the motion blur parameters using radial basis function, and use neural networks to estimate length of the blur. They use sum of Fourier coefficients as features. Authors in [5] use Artificial Neural Networks (ANN) and methods of multi-resolution decomposition of image to extract motion blur features, and use SVM (Support Vector Machines) for classification of different extent of motion blur. They demonstrate the challenges of using deep learning algorithms in de-blurring the natural images or images with compression distortions, and claim the results to have blocky, blur, and ringing artifacts. The deep learning methods find challenges in learning the features for PSF estimation. It is challenging to find distinct

features to precisely learn the extent of motion blur. To address this, we propose to score features based on the confidence generated by combining the evidences using Dempster Shafer Combination Rule (DSCR), and select the relevant features for learning. The novelty of this work lies in proposing a new way of modelling the PSF as a function of motion blur parameters (length and angle) and then using learning based framework to estimate the blur parameters. We demonstrate that our estimate of the PSF is much more accurate than SoA. Another major contribution of the work is in the technique used to select the features using evidence theory and DSCR for estimating the motion blur parameters of the PSF.

Towards this, we propose to model blur PSF as a linear function of length and angle of motion blur. We use learning based framework to estimate the length and angle to determine PSF and then deblur the image. Towards this, we make the following contributions:

- We propose to estimate PSF and model deblurred image as MRF (Markov Random Field) and use MAP (maximum *a posteriori*) estimate as the final solution. We minimize the posterior energy using graph-cut [25].
- We propose to model PSF as a function of length and angle (motion blur parameters) and use learning based framework to estimate PSF. Towards this,
 - We synthetically generate data for learning extent of motion blur using natural images.
 - We propose to use a variant of clustering and collaborative representation (CCR) of the features for learning.
 - We propose to select the relevant features for CCR based on the confidence generated using DSCR.
 - We propose to generate the confidence for different features using DSCR by combining the evidences generated using the variance in feature descriptors for motion blur with different blur parameters (length- l and angle- θ).
- We demonstrate the results on real and synthetic datasets and compare the results with different state of art methods using qualitative analysis.

2. Motion De-bluring

Typically, blurred image is modelled as a convolution of true image and the PSF, and is given by

$$g = f \otimes h + \eta \quad (1)$$

where g denotes the blurred image, f is the true image, h is PSF, and η denotes the noise (additive Gaussian noise).

In frequency domain, blurred image is modelled as multiplication of true image and Optical Transfer Function (OTF), and is given by,

$$G = FH + \eta \quad (2)$$

Where H is the PSF in frequency domain, known as OTF.

If the scene f to be captured, translates with respect to the camera at a constant velocity ($v_{relative}$) under an angle of θ_r radians with the horizontal axis in the exposure interval $[0, t_{exposure}]$, the distortion can be modelled as uni-dimensional.

We then model the length of motion l as a product of relative velocity $v_{relative}$ and the maximum exposure $t_{exposure}$. i.e.

$$l = v_{relative} \times t_{exposure} \quad (3)$$

Also the point spread function (PSF) h , for uniform motion blur can be modelled as a function of length l or L and angle θ and is given by [34], [47], [39],

$$h = \begin{cases} \frac{1}{L} if \sqrt{x^2 + y^2} \leq \frac{L}{2} \text{ and } \frac{x}{y} = -\tan\theta \\ 0 \text{ otherwise} \end{cases} \quad (4)$$

where, x and y are the independent variables defining the axes for f and g . Similarly, OTF can be given by the *sinc* function and is defined by,

$$H(u, v) = sinc(\pi L(usin\theta + vcos\theta)) \quad (5)$$

We estimate the length l and angle θ using proposed learning based framework.

We model deblurred image as MRF and use MAP estimate as the final solution. The energy function for the observation model is given by,

$$E(f|g) = \underbrace{\sum_{\forall p} D_p(f_p)}_{\text{Data term}} + \lambda \underbrace{\sum_{p,q \in N_p} V_{p,q}(f(p), f(q))}_{\text{Prior term}} \quad (6)$$

where,

$$D_p(f_p) = \sum_{\forall p} (g - hf)^2$$

and,

$$V_{p,q}(f(p), f(q)) = min(\mathcal{T}, |f(p) - f(q)|)$$

where h is blur PSF, N_p is a neighborhood term, λ is a weight given to regularization term. Data term $D_p(f_p)$ is a cost of assigning a label to a pixel, $V_{p,q}$ is a prior term which acts as a regularization term, and \mathcal{T} is a threshold and is used as a tuning parameter. However, for the cases other than the noisy observations, we find that the regularization weight λ is to be kept low to avoid over smoothing. We minimize the posterior energy using graph-cut [25].

3. Learning Based PSF Estimation

In this section, we discuss the proposed framework for restoration of blurred image by learning based PSF estimation. The framework of learning based PSF estimation for image restoration is shown in Figure 1. The framework involves generation of training data for learning motion blur, feature extraction, feature selection and feature clustering towards collaborative representation for PSF estimation, and deconvolution to obtain the de-blurred image. The training dataset is generated by synthetically adding blur to a set of un-blurred images with different blur parameters (length- l and angle- θ). The texture features are its variants are extracted towards feature selection based on the confidence generated using DSCR. The selected features undergo clustering and collaborative representation towards learning different blur parameters. The motion blur parameters of the test image (blurred image) are estimated using the trained model and the corresponding PSF is determined. The estimated PSF is then used to deblur the image in a deconvolution framework.

3.1. Generation of training dataset

Towards generation of the training dataset, a set ' K ', of 151 images covering a span of natural image distribution as described in [12] are considered. In our experiment, we synthetically generate a set of blurred images $B_i^{l,\theta}$ using different extent of blur parameters (different values of l and θ) for each image i in K . We consider l ranging between [1, 30] and θ ranging between [1, 45]. Thus, a set of $B_i^{l,\theta} = 1350$ images are generated for every i in K , collectively generating $B^{l,\theta} = 203850$ training images.

We use the set $B^{l,\theta}$ and their corresponding l and θ labels as the training data to generate a learning based model.

3.2. Feature extraction

A set F_N of texture features are considered towards selection of relevant feature set F_K (where, $F_K \in F_N$) to perform clustering and collaborative representation. These F_K features contribute to generate a codebook for estimation of l and θ of the blur kernel (PSF).

A set F_T of texture features consisting of mean (μ), variance (σ^2), standard deviation (σ_X), entropy (ϵ), smoothness (S) are extracted for every image in the training dataset $B^{l,\theta}$. Also, first order gradients(both horizontal-*FOHG* and vertical-*FOVG*) and second order gradients (both horizontal-*SOHG* and vertical-*SOVG*) are extracted for every image in the training dataset to obtain gradient vectors. We extract the texture features from each of the gradient vectors (i.e F_T from *FOVG*, *FOHG*, *SOVG*, *SOHG*) and thus collectively form a feature set F_N of 25 features for every image in the training dataset $B^{l,\theta}$.

The change in the feature descriptor for a couple of features in F_N is observed to be negligible for small variation

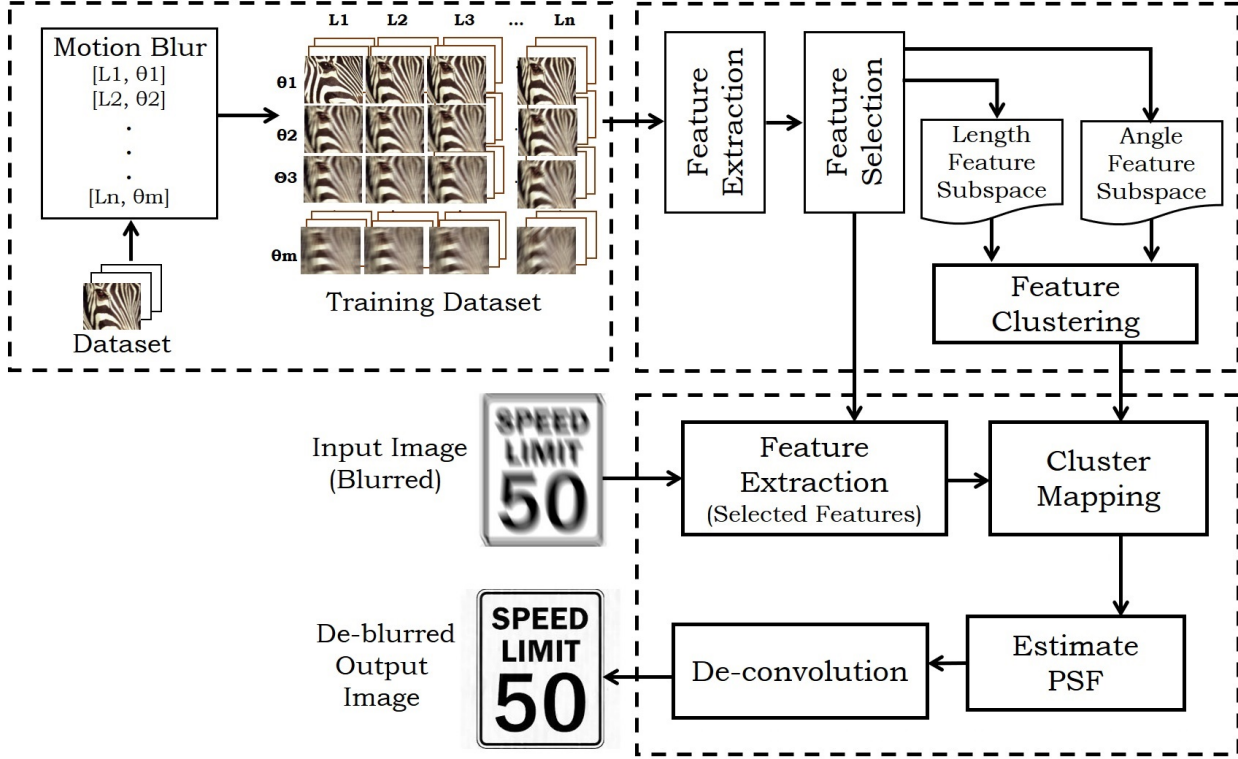


Figure 1. Framework of learning based PSF estimation for image deblurring

in blur parameters. Hence, we propose an algorithm to select a few features from F_N which can effectively contribute towards learning variation in blur parameters.

3.3. Selection of features

All the features in the feature set F_N do not contribute in learning motion-blur. Hence, it motivates to design a framework to select relevant feature set F_K from the set of features F_N . To achieve this, we propose to generate confidence C towards retention for every feature in F_N . The confidence C is estimated by combining the evidences using Dempster Shafer Combination Rule (DSCR). Every evidence is modelled as a set of masses towards belief (m_b), disbelief (m_d), uncertainty (m_u).

The features in F_N are observed to have high variation in magnitude and demands normalization as the CCR algorithm is sensitive to magnitude. Every feature in F_N is normalized to 1 using max normalization. The variance V_1 is computed amongst the feature descriptors, for the training samples with same labels. $1 - V_1$ is considered as mass of belief m_b for evidence \mathcal{E}_1 . Similarly, variance V_2 is computed amongst the feature descriptors of all the training samples generated for each un-blurred image in K . V_2 is considered as mass of belief m_b for evidence \mathcal{E}_2 . For a feature to have higher confidence C , the hypothesis is modelled such that, it is expected to have low intra-class vari-

Table 1. Dempster Shafer Combination Table [37]

\cap	$m_b(\mathcal{E}_1)$	$m_d(\mathcal{E}_1)$	$m_u(\mathcal{E}_1)$
$m_b(\mathcal{E}_2)$	ψ_1	\emptyset	ψ_1
$m_d(\mathcal{E}_2)$	\emptyset	ψ_2	ψ_2
$m_u(\mathcal{E}_2)$	ψ_1	ψ_2	Ω

ance amongst its descriptors (i.e lower value for V_1) and high inter-class variance amongst its descriptors (i.e higher value for V_2).

The mass of disbelief m_d for both the evidences \mathcal{E}_1 and \mathcal{E}_2 is considered to be 0 as we do not model a strong disbelief function towards the set hypothesis. Hence, the mass of uncertainty m_u for both the evidences \mathcal{E}_1 and \mathcal{E}_2 is considered to be $1 - m_b$.

The evidences \mathcal{E}_1 and \mathcal{E}_2 , are combined using the DSCR as demonstrated in Table 1 [37] [33]. The product of belief and disbelief gives rise to conflict, and is represented by \emptyset . The product of belief and belief, or the product of belief and uncertainty represents a component of combined belief and is represented by ψ_1 . Similarly ψ_2 represents the component of combined disbelief.

The Combined belief of the evidences \mathcal{E}_1 and \mathcal{E}_2 is considered as confidence C , and is given in the Equation 7 as

$$C = \frac{\sum \psi_1}{1 - \sum \emptyset}. \quad (7)$$

A confidence C_i is generated for every feature ‘ i ’ in F_N where $i \in N$. The features with higher confidence ($C_i > \mathcal{J}$) contribute towards formation of a reduced feature set F_K and is considered for learning. Here the threshold \mathcal{J} is set heuristically. The confidences obtained for different features are shown in Table 2 and Table 3 for varying length and varying angle respectively.

Table 2. Confidences for features on blurred dataset with constant angle θ and varying length l

Texture features	Input image (blurred)	FOHG	FOVG	SOHG	SOVG
μ	0.275	0.936	0.0082	0.538	0.0024
σ^2	0.105	0.915	0.0045	0.512	0.0022
σ_X	0.154	0.549	0.0084	0.338	0.086
ϵ	0.085	0.135	0.065	0.065	0.033
S	0.065	0.338	0.224	0.066	0.128

Table 3. Confidences for features on blurred dataset with constant length l and varying angle θ

Texture features	Input image (blurred)	FOHG	FOVG	SOHG	SOVG
μ	0.275	0.082	0.925	0.0034	0.504
σ^2	0.114	0.0459	0.935	0.013	0.543
σ_X	0.149	0.0094	0.249	0.0462	0.235
ϵ	0.081	0.035	0.235	0.033	0.065
S	0.065	0.0924	0.348	0.128	0.087

From Table 2 and Table 3 we observe, the confidence C of mean μ and variance σ^2 of first order features have higher confidence for blurred images. In Table 1, it is evident that horizontal features are relatively higher for blurred images with different length l , and in Table 3 it is evident that vertical features are relatively higher for blurred images with different angle θ . We consider these features as competent features for classification. Adding more features with high confidence may certainly improve the results, but we observe, in Table 1 and Table 3, no other features have high confidence. Adding any other feature with less confidence deteriorates the results.

We generate separate codebooks to learn length l and angle θ for the motion-blur.

3.4. Feature clustering using CCR

of mean μ and variance σ^2 of first order horizontal gradient vectors form the feature space to learn length l , and of mean μ and variance σ^2 of first order vertical gradient vectors form the feature space to learn angle θ for the motion blur. We cluster the feature space using a variant of bayes classifier, and later associate a label to every cluster

to obtain collaboratively represented codebook towards estimation of length l and angle θ .

3.5. Deconvolution/De-blurring

The mean μ and variance σ^2 of first order vertical and horizontal gradients of a test image are mapped with the separate clustered features (one for l and another for θ) to estimate length l and angle θ . The estimated length l and angle θ is used to construct the PSF (Blur kernel). The PSF and blurred image is deconvolved to obtain the de-blurred image [26]. We propose to model de-blurred image as a MRF using MAP and minimize the posterior energy using graph-cut [11]. We address the effect of local blur and variation in blurriness by performing patch based estimation of blur parameter and use the same for de-blurring. We perform graph-cut based energy minimization to overcome the artifices introduced during patch based motion blur removal, and as we perform energy minimization using graph cut, the estimation of l and θ is tolerable with an error of ± 2 units.

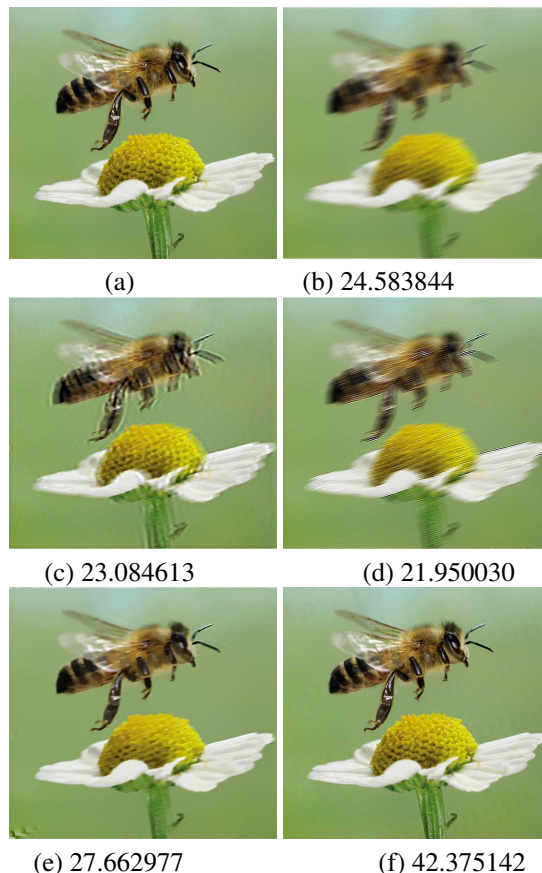


Figure 2. Results of proposed algorithm on Synthetic dataset D1: (The values indicate their corresponding PSNR with the ground truth image.) (a) ground truth image, (b) synthetically blurred image with $l = 25$ and $\theta = 18$, (c) deblurred image using [44], (d) deblurred image using [18] and (e) deblurred image using [32], (f) deblurred image using the proposed algorithm.

4. Results and Discussions

In this section, we demonstrate the results of the proposed framework on both synthetic and real datasets. We compare our results with methods proposed in [44], [18] and [32]. It is observed that the proposed method eliminates the artifacts [18] and also the ringing or block effects [32] as discussed in Section 3.5. We perform qualitative and quantitative analysis on the deblurred image obtained from the proposed framework. For quantitative analysis, we calculate RMS (Root Mean Square) error, PSNR (Peak Signal to Noise Ratio), NMI (Normalized Mutual Information) and SSIM (Structural Similarity) index of de-blurred image with the ground truth image for synthetic dataset.

4.1. Deblurring of synthetic dataset

In this section, we demonstrate the process of generation of synthetic dataset and the effect of deconvolution and optimization on deblurring. A PSF is constructed with random length l and angle θ such that $l \in [1, 30]$ and $\theta \in [1, 45]$. The un-blurred (ground truth) image ($\notin K$) is convolved with the constructed PSF to obtain a blurry image. The ground truth images are shown in Figure 2(a), Figure 3(a), and 4(a) respectively and the synthetically generated blurry images are shown in Figure 2(b), Figure 3(b), and 4(b) respectively.

The synthetically blurred images are deconvolved using the proposed framework of PSF estimation. The results are shown in Figure 2(f), Figure 3(f), and 4(f) respectively. We compare the results with the other techniques as proposed in [50], [18], [32]. The results are shown in Figure 2(c-e), Figure 3(c-e), and 4(c-e) respectively. The quality of the de blurred image obtained using the proposed framework is observed to be better than the other SOA algorithms.

For quantitative analysis, we calculate RMS (Root Mean Square) error, PSNR (Peak Signal to Noise Ratio), NMI (Normalized Mutual Information) and SSIM (Structural Similarity) index of de-blurred image with the ground truth image for synthetic dataset, and is shown in Table 4.

4.2. Deblurring of real dataset

Authors in [26] discusses about the defocus blur being space invariant. The proposed algorithm works well even if,

- Motion blur is not uniform.
- An additional defocus blur is present.

As the patch wise de-blurring addresses non-uniform motion blur, and energy minimization using graph cut addresses space invariant defocus blur, the above stated issues are addressed. It can be observed that the proposed algorithm works well for the real dataset shown in Figure 5-7(Dataset captured by moving the mobile camera in the random planar direction to introduce motion blur) which

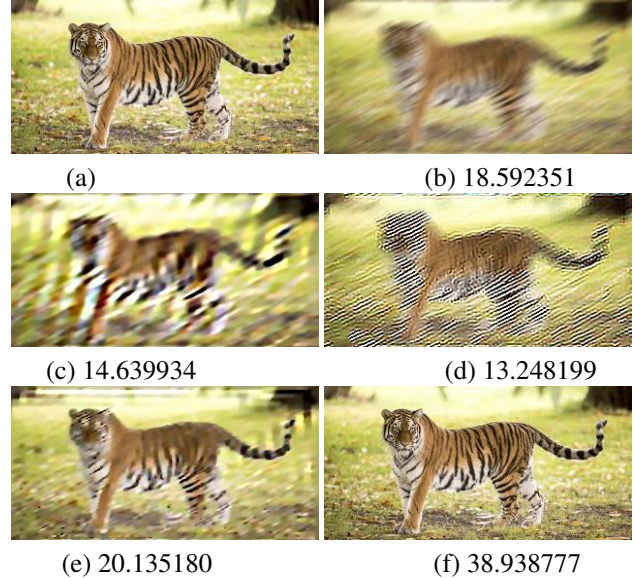


Figure 3. Results of proposed algorithm on Synthetic dataset D2: (The values indicate their corresponding PSNR with the ground truth image.) (a) ground truth image, (b) synthetically blurred image with $l = 18$ and $\theta = 27$, (c) deblurred image using [44], (d) shows the deblurred image using [18] and (e) deblurred image using [32], (f) deblurred image using the proposed algorithm.

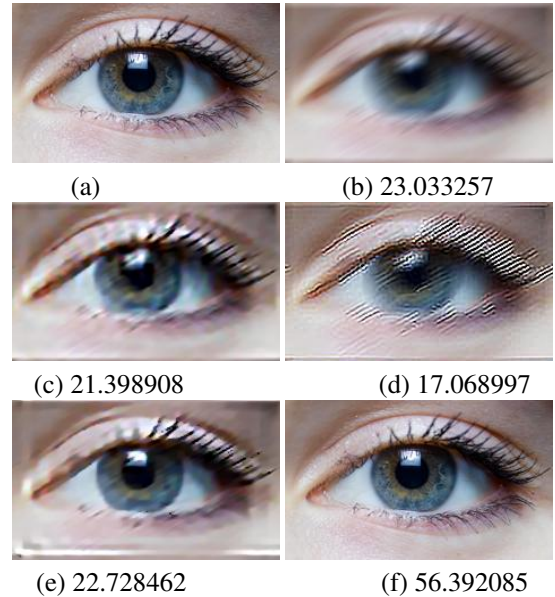


Figure 4. Results of proposed algorithm on Synthetic dataset D3: (The values indicate their corresponding PSNR with the ground truth image.) (a) ground truth image, (b) synthetically blurred image with $l = 20$ and $\theta = 30$, (c) deblurred image using [44], (d) deblurred image using [18] and (e) deblurred image using [32], (f) deblurred image using the proposed algorithm.

contains non uniform motion blur, and also space invariant defocus blur. We have evaluated the performance of our algorithm on more than 260 images of motion blur videos.

Table 4. Quality parameters for synthetic dataset. Here, RMS (Root Mean Square) error, PSNR (Peak Signal to Noise Ratio), NMI (Normalized Mutual Information) and SSIM (Structural Similarity) index of de-blurred image with the ground truth image are the quality parameters and Dataset 1 (D1) , Dataset2 (D2),Dataset 3 (D3) and Dataset 4 (D4) are the datasets used for analysis

Dataset	Image	NMI	SSIM	PSNR	RMS
D1	Blurred image	2.482705	0.914193	24.583844	15.023312
	Proposed Algorithm	11.736824	0.996997	42.375142	1.939917
	SRNID-2013 [44]	0.083126	0.888192	23.084613	17.863607
	RSBIR-2014 [18]	0.553647	0.872171	21.950030	20.363459
	IRDCP-2016 [32]	2.138787	0.945457	27.662977	10.537476
D2	Blurred image	1.474246	0.746286	18.467450	30.414169
	Proposed Algorithm	3.583922	0.997341	38.938777	2.881385
	SRNID-2013 [44]	1.238660	0.612724	14.639934	47.261623
	RSBIR-2014 [18]	1.250685	0.561964	13.248199	55.478477
	IRDCP-2016 [32]	1.598599	0.812184	20.135180	25.099777
D3	Blurred image	1.744086	0.746767	23.033257	17.983004
	Proposed Algorithm	4.117008	0.999465	56.392085	0.386310
	SRNID-2013 [44]	1.655465	0.695470	21.398908	21.704012
	RSBIR-2014 [18]	1.580482	0.588321	17.068997	35.729374
	IRDCP-2016 [32]	1.724773	0.752749	22.728462	18.625360

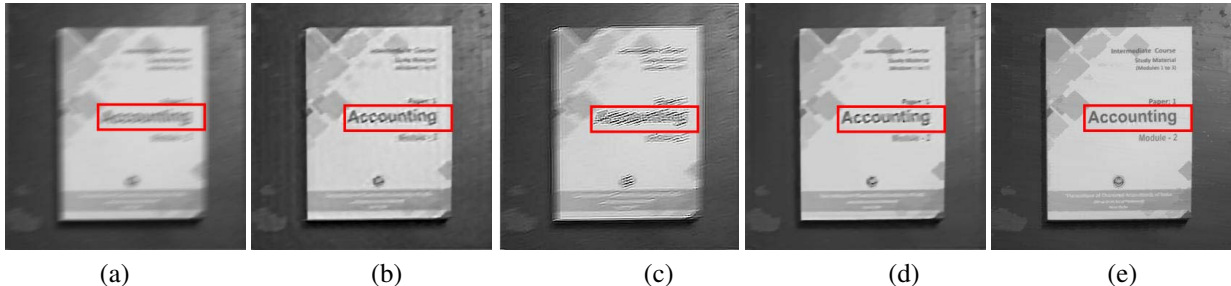


Figure 5. Results of proposed algorithm on Real dataset 1: (a) Input image, (b) deblurred image using [44], (c) deblurred image using [18] and (d) deblurred image using [32], (e) deblurred image using the proposed algorithm.

We demonstrate the algorithm on different real datasets. The results of the same are shown in Figure 5, Figure 6 and Figure 7. We perform quality analysis using the Google vision API as the ground truth is not available for quantitative analysis. We observe, no text detection in the input image or in the deblurred image using the state of art techniques. The text: “Intermediate course, Study material, Modules 1 te, Paper 1: Accounting, Module -2” being detected in the deblurred image using the proposed framework for Real dataset 1 as shown in Figure 5. We observe similar trends in the other datasets.

5. Conclusions

In this paper, we have proposed to address the problem of motion deblurring of an image by estimating Point Spread Function (PSF) using a learning-based framework. We modeled motion blur as a combination of length and angle parameters in the PSF, and proposed a learning based technique to estimate the motion blur parameters to compute the PSF. We have also proposed a technique to select the relevant features for learning based on confidence generated

by combining evidences using Dempster Shafer Combination Rule (DSCR). We have proposed to learn length and angle of motion blur by Clustering and Collaborative Representation (CCR) of feature spaces. We have proposed to model deblurred image as a MRF (Markov Random Filed) and use *MAP* (maximum a posteriori) estimate as the final solution. We have demonstrated the results on real and synthetic datasets and compared the results with different state of art methods using quality metrics and vision tools.

References

- [1] M. Cannon. Blind deconvolution of spatially invariant image blurs with phase. *IEEE Transactions on Acoustics, Speech, and Signal Processing*, 24(1):58–63, Feb 1976.
- [2] T. F. Chan and C.-K. Wong. Total variation blind deconvolution. *IEEE Transactions on Image Processing*, 7(3):370–375, Mar 1998.
- [3] M. M. Chang, A. M. Tekalp, and A. T. Erdem. Blur identification using the bispectrum. *IEEE Transactions on Signal Processing*, 39(10):2323–2325, Oct 1991.
- [4] G. Chantas, N. P. Galatsanos, R. Molina, and A. K. Katsaggelos. Variational bayesian image restoration with a

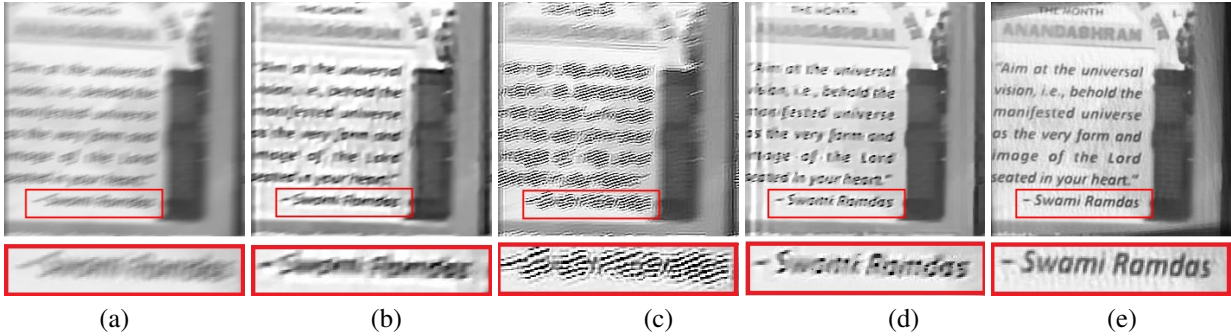


Figure 6. Results of proposed algorithm on Real dataset 2: (a) Input image, (b) deblurred image using [44], (c) deblurred image using [18] and (d) deblurred image using [32], (e) deblurred image using the proposed algorithm.

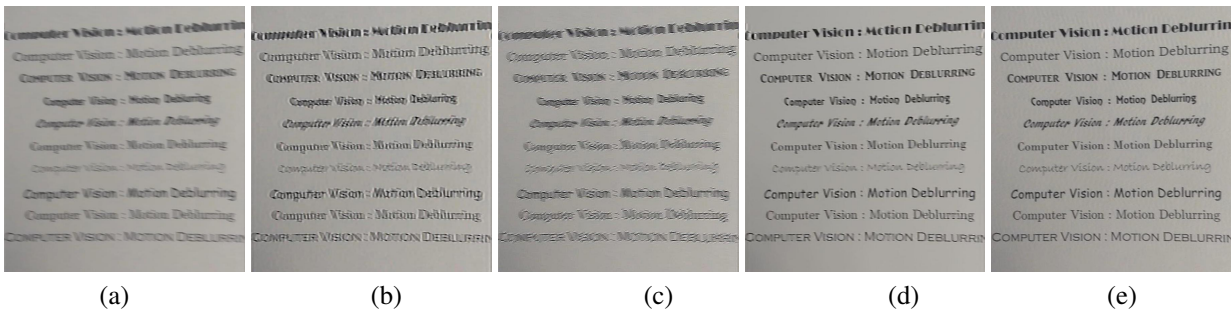


Figure 7. Results of proposed algorithm on Real dataset 3: (a) Input image, (b) deblurred image using [44], (c) deblurred image using [18] and (d) deblurred image using [32], (e) deblurred image using the proposed algorithm.

- product of spatially weighted total variation image priors. *IEEE Transactions on Image Processing*, 19(2):351–362, Feb 2010.
- [5] M. J. Chen and A. C. Bovik. No-reference image blur assessment using multiscale gradient. In *2009 International Workshop on Quality of Multimedia Experience*, pages 70–74, July 2009.
 - [6] X. Chen, X. He, J. Yang, and Q. Wu. An effective document image deblurring algorithm. In *CVPR 2011*, pages 369–376, June 2011.
 - [7] D. G. Childers, D. P. Skinner, and R. C. Kemerait. The cepstrum: A guide to processing. *Proceedings of the IEEE*, 65(10):1428–1443, Oct 1977.
 - [8] H. Cho, J. Wang, and S. Lee. Text image deblurring using text-specific properties. In *Proceedings of the 12th European Conference on Computer Vision - Volume Part V, ECCV’12*, pages 524–537, Berlin, Heidelberg, 2012. Springer-Verlag.
 - [9] S. Cho and S. Lee. Fast motion deblurring. In *ACM SIGGRAPH Asia 2009 Papers, SIGGRAPH Asia ’09*, pages 145:1–145:8, New York, NY, USA, 2009. ACM.
 - [10] R. Dash, P. K. Sa, and B. Majhi. Rbf based motion blur parameter estimation. In *2009 International Conference on Advanced Computer Control*, pages 327–331, Jan 2009.
 - [11] R. R. Dhanakshirur, P. Pillai, R. A. Tabib, U. Patil, and U. Mudanagudi. A framework for lane prediction on unstructured roads. In *International Symposium on Signal Processing and Intelligent Recognition Systems*, pages 178–189. Springer, 2018.
 - [12] C. Dong, C. C. Loy, K. He, and X. Tang. Image super-resolution using deep convolutional networks. *IEEE Transactions on Pattern Analysis and Machine Intelligence*, 38(2):295–307, Feb 2016.
 - [13] W. Dong, L. Zhang, G. Shi, and X. Li. Nonlocally centralized sparse representation for image restoration. *IEEE Transactions on Image Processing*, 22(4):1620–1630, April 2013.
 - [14] R. Fabian and D. Malah. Robust identification of motion and out-of-focus blur parameters from blurred and noisy images. *CVGIP: Graph. Models Image Process.*, 53(5):403–412, July 1991.
 - [15] X. Fang, H. Wu, Z. Wu, and B. Luo. An improved method for robust blur estimation. 10:1709–1716, 09 2011.
 - [16] R. Fergus, B. Singh, A. Hertzmann, S. T. Roweis, and W. T. Freeman. Removing camera shake from a single photograph. In *ACM SIGGRAPH 2006 Papers, SIGGRAPH ’06*, pages 787–794, New York, NY, USA, 2006. ACM.
 - [17] Z. Hu, S. Cho, J. Wang, and M. H. Yang. Deblurring low-light images with light streaks. In *2014 IEEE Conference on Computer Vision and Pattern Recognition*, pages 3382–3389, June 2014.
 - [18] A. Kheradmand and P. Milanfar. A general framework for regularized, similarity-based image restoration. *IEEE Transactions on Image Processing*, 23(12):5136–5151, Dec 2014.
 - [19] F. Kraemer, Y. Lin, B. McAdoo, K. Ott, J. Wang, D. Widemann, and B. Wohlberg. Blind image deconvolution motion blur estimation. 07 2008.
 - [20] D. Krishnan, T. Tay, and R. Fergus. Blind deconvolution using a normalized sparsity measure. In *CVPR 2011*, pages 233–240, June 2011.
 - [21] S. Lefkimmiatis, A. Bourquard, and M. Unser. Hessian-based norm regularization for image restoration with

- biomedical applications. *IEEE Transactions on Image Processing*, 21(3):983–995, March 2012.
- [22] A. Levin, Y. Weiss, F. Durand, and W. T. Freeman. Understanding and evaluating blind deconvolution algorithms. In *2009 IEEE Conference on Computer Vision and Pattern Recognition*, pages 1964–1971, June 2009.
- [23] A. Levin, Y. Weiss, F. Durand, and W. T. Freeman. Efficient marginal likelihood optimization in blind deconvolution. In *CVPR 2011*, pages 2657–2664, June 2011.
- [24] T. Michaeli and M. Irani. Blind deblurring using internal patch recurrence. 8691:783–798, 09 2014.
- [25] U. Mudenagudi, S. Banerjee, and P. K. Kalra. Space-time super-resolution using graph-cut optimization. *IEEE Transactions on Pattern Analysis and Machine Intelligence*, 33(5):995–1008, May 2011.
- [26] U. Mudenagudi, S. Banerjee, and P. K. Kalra. Space-time super-resolution using graph-cut optimization. *IEEE Transactions on Pattern Analysis and Machine Intelligence*, 33(5):995–1008, 2011.
- [27] R. Neelamani, H. Choi, and R. Baraniuk. Forward: Fourier-wavelet regularized deconvolution for ill-conditioned systems. *IEEE Transactions on Signal Processing*, 52(2):418–433, Feb 2004.
- [28] J. Ni, P. Turaga, V. M. Patel, and R. Chellappa. Example-driven manifold priors for image deconvolution. *IEEE Transactions on Image Processing*, 20(11):3086–3096, Nov 2011.
- [29] J. Oliveira, J. Bioucas-Dias, and M. Figueiredo. Adaptive total variation image deblurring: A majorization–minimization approach. 89:1683–1693, 09 2009.
- [30] J. Pan, Z. Hu, Z. Su, and M.-H. Yang. Deblurring face images with exemplars. pages 47–62, 09 2014.
- [31] J. Pan, Z. Hu, Z. Su, and M. H. Yang. Deblurring text images via l0-regularized intensity and gradient prior. In *2014 IEEE Conference on Computer Vision and Pattern Recognition*, pages 2901–2908, June 2014.
- [32] J. Pan, D. Sun, H. Pfister, and M. H. Yang. Blind image deblurring using dark channel prior. In *2016 IEEE Conference on Computer Vision and Pattern Recognition (CVPR)*, pages 1628–1636, June 2016.
- [33] U. Patil, R. A. Tabib, C. M. Konin, and U. Mudenagudi. Evidence-based framework for multi-image super-resolution. In *Recent Findings in Intelligent Computing Techniques*, pages 413–423. Springer, 2018.
- [34] I. Rekleitis. *Visual motion estimation based on motion blur interpretation*. PhD thesis, Citeseer, 1995.
- [35] I. Rekleitis. Steerable filters and cepstral analysis for optical flow calculation from a single blurred image. 03 1999.
- [36] Q. Shan, J. Jia, and A. Agarwala. High-quality motion deblurring from a single image. *ACM Transactions on Graphics (SIGGRAPH)*, 2008.
- [37] R. A. Tabib, U. Patil, S. A. Ganihar, N. Trivedi, and U. Mudenagudi. Decision fusion for robust horizon estimation using dempster shafer combination rule. In *2013 Fourth National Conference on Computer Vision, Pattern Recognition, Image Processing and Graphics (NCVPRIPG)*, pages 1–4, Dec 2013.
- [38] H. Takeda, S. Farsiu, and P. Milanfar. Deblurring using regularized locally adaptive kernel regression. *IEEE Transactions on Image Processing*, 17(4):550–563, April 2008.
- [39] S. Tiwari, V. Shukla, S. Biradar, and A. Singh. Blur parameters identification for simultaneous defocus and motion blur. *CSI transactions on ICT*, 2(1):11–22, 2014.
- [40] H. Tong, M. Li, H. Zhang, and C. Zhang. Blur detection for digital images using wavelet transform. In *2004 IEEE International Conference on Multimedia and Expo (ICME) (IEEE Cat. No.04TH8763)*, volume 1, pages 17–20 Vol.1, June 2004.
- [41] Y. Wang, J. Yang, W. Yin, and Y. Zhang. A new alternating minimization algorithm for total variation image reconstruction. *SIAM Journal on Imaging Sciences*, 1(3):248–272, 2008.
- [42] C.-H. Wu, k.-k. Tseng, C.-K. Ng, and W. Ip. An effective motion-blurred image restoration approach for automated optical inspection. 22:252–262, 10 2015.
- [43] L. Xu and J. Jia. Two-phase kernel estimation for robust motion deblurring. In *Proceedings of the 11th European Conference on Computer Vision: Part I, ECCV’10*, pages 157–170, Berlin, Heidelberg, 2010. Springer-Verlag.
- [44] L. Xu, S. Zheng, and J. Jia. Unnatural l0 sparse representation for natural image deblurring. In *2013 IEEE Conference on Computer Vision and Pattern Recognition*, pages 1107–1114, June 2013.
- [45] Z. Yang and M. Jacob. Nonlocal regularization of inverse problems: A unified variational framework. *IEEE Transactions on Image Processing*, 22(8):3192–3203, Aug 2013.
- [46] Y. Ye, X. Pan, and J. Wang. Identification of blur parameters of motion blurred image using fractional order derivative. In *2012 11th International Conference on Information Science, Signal Processing and their Applications (ISSPA)*, pages 539–544, July 2012.
- [47] Y. Yitzhaky and N. S. Kopeika. Identification of blur parameters from motion blurred images. *Graphical models and image processing*, 59(5):310–320, 1997.
- [48] Y. Yoshida, K. Horiike, and K. Fujita. Parameter estimation of uniform image blur using dct. pages 1154–1157, 07 1993.
- [49] L. Yuan, J. Sun, L. Quan, and H.-Y. Shum. Progressive inter-scale and intra-scale non-blind image deconvolution. *ACM Trans. Graph.*, 27(3):74:1–74:10, Aug. 2008.
- [50] H. Zhang, D. Wipf, and Y. Zhang. Multi-image blind deblurring using a coupled adaptive sparse prior. In *2013 IEEE Conference on Computer Vision and Pattern Recognition*, pages 1051–1058, June 2013.
- [51] X. Zhang, M. Burger, X. Bresson, and S. Osher. Bregmanized nonlocal regularization for deconvolution and sparse reconstruction. *SIAM Journal on Imaging Sciences*, 3(3):253–276, 2010.